Kv Channel Gating Requires a Compatible S4-S5 Linker and Bottom Part of S6, Constrained by Non-interacting Residues

Alain J. Labro,[1] Adam L. Raes,[1] Alessandro Grottesi,[2] Diane Van Hoorick,[1] Mark S.P. Sansom,[3] and Dirk J. Snyders[1]

[1]Laboratory for Molecular Biophysics, Physiology, and Pharmacology, Department of Biomedical Sciences, University of Antwerp, 2610 Antwerp, Belgium
[2]Consorzio Interuniversitario per le Applicazioni del Supercalcolo per Universita e Ricerca (CASPUR), 00185 Rome, Italy
[3]Laboratory for Molecular Biophysics, Department of Biochemistry, University of Oxford, Oxford OX1 4BH, England, UK

Voltage-dependent K^+ channels transfer the voltage sensor movement into gate opening or closure through an electromechanical coupling. To test functionally whether an interaction between the S4-S5 linker (L45) and the cytoplasmic end of S6 ($S6_T$) constitutes this coupling, the L45 in hKv1.5 was replaced by corresponding hKv2.1 sequence. This exchange was not tolerated but could be rescued by also swapping $S6_T$. Exchanging both L45 and $S6_T$ transferred hKv2.1 kinetics to an hKv1.5 background while preserving the voltage dependence. A one-by-one residue substitution scan of L45 and $S6_T$ in hKv1.5 further shows that $S6_T$ needs to be α-helical and forms a "crevice" in which residues I422 and T426 of L45 reside. These residues transfer the mechanical energy onto the $S6_T$ crevice, whereas other residues in $S6_T$ and L45 that are not involved in the interaction maintain the correct structure of the coupling.

INTRODUCTION

Voltage-gated potassium channels (Kv channels) are composed of four α-subunits, each containing six membrane-spanning helices (S1-S6) with a pore loop between S5 and S6 that forms the ion selectivity filter. The four subunits line the rest of the ion-conducting pathway primarily by their hydrophobic S6 segments. The S4 segment forms the main part of the channel's voltage-sensing domain (VSD) that reorients upon a change in the membrane potential (for review see Bezanilla, 2000). This reorientation subsequently triggers the opening or closing of the activation gate, which is located at the lower end of S6 (Liu et al., 1997; del Camino and Yellen, 2001). It is still not fully understood how the voltage sensor is physically coupled to the channel gate. One hypothesis states that the S4 movement pulls or twists the cytoplasmic S4-S5 linker that is coupled to the bottom of the S6 segment. Interactions between the S4-S5 linker and the C-terminal end of S6 have been proposed in hERG and HCN channels (Tristani-Firouzi et al., 2002; Decher et al., 2004; Ferrer et al., 2006). In the case of *Shaker* and KcsA, chimeric constructs were functional only when the chimera contained both the sequence of the S4-S5 linker and the cytoplasmic end of S6 from *Shaker* (Lu et al., 2002; Caprini et al., 2005). The 3-D crystal structure of the mammalian *Shaker*-type channel rKv1.2 strengthened this hypothesis as it supported an interaction between the bottom part of S6 and the S4-S5 linker (Long et al., 2005b). However, as channel gating is a process that involves several movements (rotation, translation, and tilting), the coupling mechanism is a dynamic process that likely involves multipoint interactions that need not be the same in the open and closed state.

Mutations in the C-terminal S6 end of *Shaker* and hKv1.5 altered both channel gating and the stability of the activation gate, strengthening the role of this section in channel gating (Hackos et al., 2002; Rich et al., 2002). Furthermore, cysteine substitutions in the $S6_T$ region (tail end of S6 and the beginning of the C-terminal region, named as in Ding and Horn, 2002) of *Shaker* altered the single-channel conductance and affected gating currents (Ding and Horn, 2002; Ding and Horn, 2003). To evaluate whether the important residues in $S6_T$ of hKv1.5 matched those within the rKv1.2 crystal structure, we preformed a glycine and alanine substitution scan and made selected proline mutations. To characterize further the residues that constitute the electromechanical coupling, we first replaced in an hKv1.5 background the S4-S5 linker (abbreviated as L45 throughout) and/or the $S6_T$ region by the corresponding hKv2.1 sequence. Subsequently, we substituted selected residues individually and interpreted the

Correspondence to Dirk J. Snyders: dirk.snyders@ua.ac.be

Abbreviations used in this paper: VSD, voltage-sensing domain; WT, wild-type.

The online version of this article contains supplemental material.

The Rockefeller University Press $30.00
J. Gen. Physiol. Vol. 132 No. 6 667–680
www.jgp.org/cgi/doi/10.1085/jgp.200810048

results using an hKv1.5 homology model based on the rKv1.2 crystal structure (Long et al., 2005a). The results suggest that both L45 and $S6_T$ adopt an α-helical structure and that at least two groups of residues can be identified as critical for gating: residues that physically transduce the mechanical energy and residues that keep the correct interface intact.

MATERIALS AND METHODS

Molecular Biology

Mutations were introduced in hKv1.5 in a pBK-CMV expression vector using the QuikChange site-directed mutagenesis kit (Agilent Technologies) and mutant primers. After the PCR-based mutagenesis, the fragment containing the mutation was cut out of the PCR-amplified vector and ligated in hKv1.5/pBK-CMV to replace the wild-type (WT) sequence. Double-stranded sequencing of the exchanged fragment and the adjacent sequence confirmed the presence of the desired modification and the absence of unwanted mutations. Plasmid DNA for mammalian expression was obtained by amplification in XL2 blue script cells (Agilent Technologies) and harvested using the GenElute HP plasmid maxiprep kit (Sigma-Aldrich). The cDNA concentration was determined with UV absorption.

Electrophysiology

Ltk^- cells were cultured in DMEM medium supplemented with 10% horse serum and 1% penicillin/streptomycin. The cells were transiently transfected with 1–5 µg cDNA for WT or mutant subunits using polyethyleneimine (Sigma-Aldrich) (Boussif et al., 1995). 1–5 µg cDNA was mixed with 5 µl of a 1-mg polyethyleneimine/ml stock solution and was added to 100 µl DMEM medium. After a 15-min incubation at room temperature, the mixture was added to the cells in a culture dish that had a cell confluency of ∼60%. 16–24 h after transfection the cells were trypsinized and used for analysis within 12 h. Current recordings were done at room temperature (21–23°C) with an Axopatch-200B amplifier (MDS Analytical Technologies) in the whole cell configuration and digitized with a Digidata-1200A data acquisition system (MDS Analytical Technologies). Command voltages and data storage were controlled with pClamp8 software (MDS Analytical Technologies). Patch pipettes were pulled from 1.2-mm quick-fill borosilicate glass capillaries (World Precision Instruments) with a P-2000 puller (Sutter Instrument Co.) and heat polished. The cells were perfused continuously with a bath solution containing (in mM) 130 NaCl, 4 KCl, 1.8 $CaCl_2$, 1 $MgCl_2$, 10 HEPES, and 10 glucose, adjusted to pH 7.35 with NaOH. The pipettes solution contained (in mM) 110 KCl, 5 K_4BAPTA, 5 K_2ATP, 1 $MgCl_2$, and 10 HEPES, adjusted to pH 7.2 using KOH. Junction potentials were zeroed with the filled pipette in the bath solution. The remaining liquid junction potential was not corrected and estimated to be 1.7 mV. Experiments were excluded from analysis if the voltage errors originating from series resistance exceeded 5 mV after compensation.

Data Analysis

The holding potential was −80 mV, and the interpulse interval was at least 15 s but was increased to 25 s for some protocols to prevent the accumulation of slow inactivation. Voltage protocols were adjusted to characterize the biophysical properties of mutant channels adequately. Time constants of activation and deactivation were determined from fitting a single or double exponential function to the recorded currents. The voltage dependence of activation and inactivation was fitted with a Boltzmann function: $y = 1/(1+\exp[-(E-V_{1/2})/k])$, where E is the applied voltage, $V_{1/2}$ the midpoint potential, and k the slope factor. Results are expressed as mean ± SEM, with *n* the number of cells analyzed.

Confocal Imaging

To determine cell surface expression, we introduced a HA tag into the S1-S2 loop of WT hKv1.5 and mutants by a loop-in PCR reaction with primers containing the coding sequence for the tag. Ltk^- cells were cultivated on coverslips and transfected following the lipofection method using lipofectAMINE (Invitrogen).4 µg channel cDNA was cotransfected with 0.5 µg DsRed ER localization vector that allowed us to visualize the ER without the need of an antibody. Two semi-confluent coverslips were transfected in parallel. After 18 h of incubation, the cells were washed and fixed with 4% paraformaldehyde. The cells of one coverslip were permeabilized with 0.1% Triton X-100 (Sigma-Aldrich), the other not. Subsequently, cells were stained with rat anti-HA (Roche) followed by anti–rat FITC (Sigma-Aldrich) antibody. Confocal images were obtained on a Zeiss CLSM 510 equipped with an argon laser (excitation 488 nm) and a Helium-Neon laser (excitation 543 nm) for the single-track visualization of FITC and DsRed-ER.

Homology Model

The hKv1.5 pore domain was homology modeled using Modeller (Sali and Blundell, 1993) and the channel x-ray structure of rKv1.2 (PDB code 2A79) as a template (Long et al., 2005a). Sequence alignment of the target sequence was generated using ClustalX. 50 homology models were generated and scored against the minimum number of constraint violations. Among them, the five lowest energy models were selected and analyzed using Procheck (Laskowski et al., 1993). The final model was chosen according to the highest percentage of residues in the allowed region of the Ramachandran plot (>90%).

The interaction between $S6_T$ and L45 was studied by optimizing the interaction among residues located on the contacting surface of these segments. Thus, we restricted our calculations to the S6 helix and S4-S5 linker alone. The L45 was manually moved upwards to position I422 and T426 at contact distance to F519 and F522, respectively. This distorted model was optimized by performing a 1,000-step conjugate gradient minimization, followed by a 10,000-step molecular dynamics simulation in vacuo at 300 K with constant volume. The CHARMM19 force field was used with package NAMD 2.6 (Phillips et al., 2005). Energetic analysis was performed using the NAMD energy module in the VMD package (Humphrey et al., 1996). The space-fill representations of the S6 and S4-S5 linker interaction has been rendered by calculating the solvent-accessible surface with MSMS (Sanner et al., 1996) using a probe radius of 1.4 Å and visualized with VMD 1.8.6.

Online Supplemental Material

The subcellular localization of chimeric channel constructs and the detailed biophysical properties of substitution mutants of important L45 residues are shown in Figs. S1 and S2, respectively. The structural implications of substituting residues F519, F522, and Y523 in the $S6_T$ region by an alanine or a leucine are shown in Fig. S3. The coordinates of the hKv1.5 homology model that was generated as well as the coordinates of the hypothetical model of the coupling are also available as PDB files. The online supplemental material is available at http://www.jgp.org/cgi/content/full/jgp.200810048/DC1.

RESULTS

Alanine/Glycine Substitution Scan in the Bottom Part of S6

It has been suggested that the $S6_T$ region is involved in channel gating of *Shaker*-type channels (Ding and Horn,

2002; Hackos et al., 2002; Rich et al., 2002; Ding and Horn, 2003). The 3-D crystal structure of rKv1.2 strengthened this hypothesis and showed a possible coupling with the S4-S5 linker (Long et al., 2005b). To evaluate the structure of the $S6_T$ region and to investigate the contribution of each residue in channel gating, we replaced residues 515–527 in hKv1.5 individually by glycine or alanine (Table I). Because of the lack of a side chain, glycine has a large degree of freedom of rotation about the phi psi dihedral angles and can introduce conformational flexibility (O'Neil and DeGrado, 1990; Blaber et al., 1993) in case the $S6_T$ region would not be α-helical. However, to exclude the possibility that glycine substitutions would not be tolerated because of their α-helical destabilizing ability, we also performed an alanine substitution scan. An alanine has likewise a

TABLE I

Substitution Scan of the C-terminal Part of S6

hKv1.5	V	P	V	I	V	S	N	F	N	Y	F	Y	H	R	E	T	D
		I		I		I		I		I		I		I		I	
position		513		515		517		519		521		523		525		527	
		(475)		(477)		(479)		(481)		(483)		(485)		(487)		(489)	
				Activation						Deactivation				Inactivation			
		$V_{1/2}$ (mV)		k (mV)		τ_a (ms)				τ_d (ms)			$V_{1/2,i}$ (mV)			k_i (mV)	*n*
hKv1.5		−14.3 ± 1.0		5.8 ± 0.2		3.5 ± 0.2				24.9 ± 2.5			−23.2 ± 1.3			3.9 ± 0.1	8
I515G		no current															5
V516G		no current															9
S517G		0.3 ± 1		6.4 ± 0.4		5.1 ± 0.7				31.9 ± 3.5			−8.3 ± 1.3			4.6 ± 0.3	6
N518G		no current															8
F519G		no current															14
N520G		2.8 ± 1.7		6.7 ± 0.3		6.9 ± 0.5				21.4 ± 3.9			−6.6 ± 1.4			4.6 ± 0.2	7
Y521G		>28		>32		13.0 ± 0.9				18.6 ± 3.1			−18.7 ± 1.5			4.4 ± 0.4	4
F522G		no current															9
Y523G		no current															16
H524G		−9.8 ± 2		6.9 ± 0.4		6.5 ± 1.0				23.5 ± 1.5			−18.5 ± 2.7			5.1 ± 0.3	5
R525G		−5.9 ± 1.7		6.9 ± 0.5		6.3 ± 0.6				11.8 ± 1.2			−15.7 ± 1.3			4.0 ± 0.3	5
E526G		−0.7 ± 1.5		5.7 ± 0.3		3.3 ± 0.2				11.1 ± 0.8			−7.8 ± 1.4			4.6 ± 0.3	7
T527G		5.5 ± 1.7		6.4 ± 0.4		4.9 ± 0.5				12.7 ± 0.9			0.8 ± 2.2			5.1 ± 0.5	6
I515A		no current															6
V516A		−7.3 ± 1.8		6.0 ± 0.3		4.0 ± 0.6				3.6 ± 0.3			−11.6 ± 1.8			3.8 ± 0.2	7
S517A		−1.1 ± 1.5		6.7 ± 0.2		5.3 ± 1.0				26.0 ± 3.2			−11.6 ± 1.2			4.9 ± 0.1	6
N518A		no current															9
F519A		no current															8
N520A		−5.2 ± 1.4		6.9 ± 0.3		4.3 ± 0.3				38.4 ± 0.9			−15.3 ± 0.5			4.8 ± 0.3	6
Y521A		−16.6 ± 1.3		5.4 ± 0.3		3.3 ± 0.2				5.0 ± 0.4			−20.4 ± 1.1			3.9 ± 0.2	5
F522A		no current															11
Y523A		no current															16
H524A		−16.1 ± 1.6		6.7 ± 0.4		5.6 ± 0.4				33.7 ± 5.2			−25.2 ± 1.9			4.3 ± 0.2	7
R525A		−14.0 ± 1.3		6.1 ± 0.4		5.1 ± 0.7				31.2 ± 3.8			−23.9 ± 1.3			4.1 ± 0.3	6
E526A		−15.0 ± 1.2		6.7 ± 0.5		4.6 ± 0.5				18.7 ± 2.3			−23.1 ± 1.1			4.3 ± 0.1	8
T527A		−5.0 ± 2.2		6.6 ± 0.6		7.1 ± 1.5				21.4 ± 2.8			−11.8 ± 1.2			4.6 ± 0.4	5
V516P		no current															5
S517P		no current															7
N520P		no current															7
Y521P		no current															5
F519L		no current															5
F522L		−20.6 ± 3.2		5.2 ± 0.6		3.3 ± 0.3				32.8 ± 3.9			−28.1 ± 2.9			3.6 ± 0.1	5
Y523L		−22.8 ± 2.2		5.5 ± 0.5		3.6 ± 0.3				145 ± 18			−31.7 ± 0.9			3.7 ± 0.2	6

On top the sequence of the $S6_T$ region of hKv1.5. The mutations are represented with the residue numbering of hKv1.5. Midpoint of activation ($V_{1/2}$) and slope factor of activation (k) were calculated as described in Materials and methods. The time constants of activation (τ_a) and deactivation (τ_d) were obtained at $V_{1/2}$ +60 mV and $V_{1/2}$ −40 mV, respectively. In the case of Y521G, the $V_{1/2}$ was too positive and the slope too shallow to be determined by curve fitting, precluding an accurate estimate. For Y521G, the time constant of activation and deactivation was obtained at +80 mV and −30 mV. Midpoint of inactivation ($V_{1/2,i}$) and slope factor (k_i) were obtained from the reduction of current during a step to +50 mV after a 5-s prepulse to voltages between −80 and +20 mV.

small side chain but in contrast acts as an α-helix promoter (O'Neil and DeGrado, 1990; Blaber et al., 1993). If neither an alanine nor glycine substitution would be tolerated, this would indicate the loss of an important side chain (interaction).

The individual replacement of residues S517, N520, Y521, H524, R525, E526, and T527 by a glycine or an alanine resulted in functional channels (Table I). With the exception of Y521G, the voltage dependence of activation of these mutants was similar to WT or slightly shifted toward positive potentials (Table I). The activation curve of the Y521G mutant did not reach full saturation within the voltage range of −40 to +100 mV, but the apparent threshold for activation was similar to WT (Fig. 1). As a result, the voltage dependence of activation was very shallow with a midpoint potential positive to +28 mV and a slope factor of at least 32 mV. hKv1.5 displays slow and partial C-type inactivation; with 5-s steps the isochronal inactivation curve is characterized by a midpoint of −23.2 ± 1.3 mV ($n = 8$) and a slope factor of 3.9 ± 0.1 mV. Apparently, the inactivation curve of Y521G did reach saturation and displayed a small shift toward negative potentials compared with WT (Fig. 1). The activation and deactivation time constants were for all functional mutants similar to WT, except for Y521G, which activated approximately four times slower than WT (Table I). In contrast, the Y521A mutation resulted in channels with activation kinetics that resembled WT but with deactivation time constants that were approximately five times faster (Table I). On the other hand,

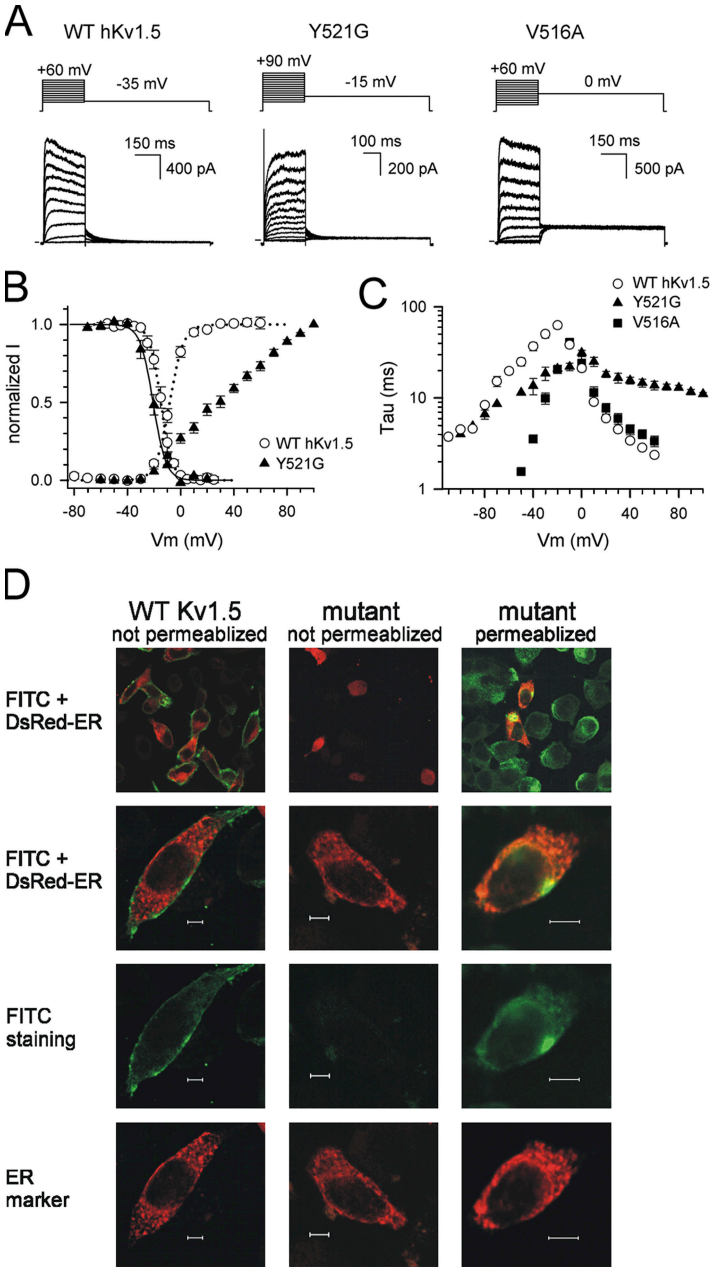

Figure 1. Biophysical properties and subcellular localization of WT hKv1.5 and selected channel mutants. (A) Current tracings for WT hKv1.5 and $S6_T$ mutants Y521G and V516A with the voltage protocol used on top. The horizontal bar on the left indicates the zero current level. (B) The voltage dependence of activation and inactivation of both WT hKv1.5 (open circles) and the mutant Y521G (filled triangles). Normalized current amplitudes were plotted as a function of the prepulse potential. Note that the voltage dependence of inactivation was normalized between 0 and 1, but the extent of inactivation after 5-s depolarizations was 58 ± 5% ($n = 7$) and 54 ± 9% ($n = 4$) for WT and Y521G, respectively. Values are expressed as mean ± SEM. (C) The activation and deactivation time constants of WT hKv1.5 (circles), Y521G (triangles), and V516A (squares). Note that V516A, which displayed a voltage dependence of activation and inactivation like WT, deactivated clearly faster than WT, although the activation time constants were comparable. (D) Confocal images of WT hKv1.5 and the nonfunctional channel mutant F522G. Subcellular localization was determined with immunocytochemistry with HA antibody against HA tag in the S1S2 loop. In the left column, confocal images from nonpermeabilized WT hKv1.5–expressing cells are shown. In the middle and right columns, images from cells that express the mutant F522G before and after permeabilization, respectively, are shown. The top panels show an overview image containing several cells. The panels below are a confocal image of a typical cell. In all the detailed panels, a scale bar of 5 μm is shown. For WT, there was a prominent FITC (green fluorescence) membrane staining with a proper ER coloring (red fluorescence). The FITC membrane staining indicated that channels were expressed at the level of the cell membrane. Note that the images were obtained from nonpermeabilized cells. The cells expressing the nonfunctional channel mutant F522G in the middle column were not permeabilized and displayed no FITC staining (no green fluorescence), although ER marking (red fluorescence) indicated that the cells were properly transfected. In contrast, the permeabilized cells displayed a clear intracellular FITC staining (right column of images). The yellow-brown overlap between the red (ER) and green fluorescence (channel subunits) indicated that the subunits were synthesized but retained in the ER and did not reach the cell membrane. All nonfunctional mutants showed a staining pattern similar to that of the F522G mutant.

alanine or glycine substitutions of residues I515, N518, F519, F522, and Y523 were not tolerated, as no time-dependent current activation was observed within the voltage range of −130 to +130 mV with up to 7 μg cDNA transfected (that yields currents >20 nA for WT). Position V516 formed an exception as an alanine substitution resulted in functional channels, but this was not the case for the glycine substitution (Table I and Fig. 1).

To determine if nonfunctionality resulted from misfolded channel proteins that did not pass the ER quality control, the plasma membrane expression of WT and nonfunctional channel mutants was determined with immunocytochemistry using constructs that contained an HA tag in the S1-S2 loop. Confocal imaging showed that WT displayed prominent membrane staining, whereas the nonfunctional glycine mutant F522G did not (Fig. 1). The success of the cell transfection was verified by the ER fluorescence of the DsRed ER marker. Furthermore, a clear intracellular staining was observed upon membrane permeabilization, indicating that the F522G mutant channels were synthesized but did not reach the cell surface. The other nonfunctional substitution mutants all showed similar results as for the F522G mutant (not depicted).

Altogether, between residue positions 515 and 527, the positions where glycine or alanine substitutions were tolerated or not coincided, and the periodicity matched an α-helical structure (Fig. 2 A). As a consequence, disrupting the α-helical structure may result in nonfunctionality. This was tested with selected proline substitutions, as a proline residue tends to destabilize an α-helical structure due to folding constraints (MacArthur and Thornton, 1991). The individual proline substitution of residues S517, N520, and Y521 that tolerated both alanine and glycine substitution, as well as V516 that only tolerated the alanine substitution, were indeed not tolerated.

To interpret the structural repercussions of the substitution mutants, a rKv1.2-based homology model was generated for hKv1.5, as described in Materials and methods. In this model, the side chain of residue F519 is directed almost perpendicular to the axis of both $S6_T$ and the S4-S5 linker (L45) (Fig. 2). In contrast, the side chains of F522 and Y523 are positioned at an angle of ∼60° with the $S6_T$ axis, thus protruding less. Therefore, we hypothesized that a bulky non-aromatic residue might substitute for F522 and Y523, but not for F519. Indeed, F522L and Y523L generated voltage-dependent K^+ currents, whereas F519L did not, likely because a leucine is not bulky enough to substitute for F519. Both functional mutants shifted the voltage dependence of activation and inactivation toward negative potentials compared with WT (Table I). The channel kinetics were comparable to WT except for the deactivation of Y522L, which were approximately six times slower (Table I).

Exchanging L45 and $S6_T$ in hKv1.5 by hKv2.1 Sequence

To identify the molecular determinants of the coupling between the S4-S5 linker and the $S6_T$, all residues that could be responsible for this contact in Kv channels

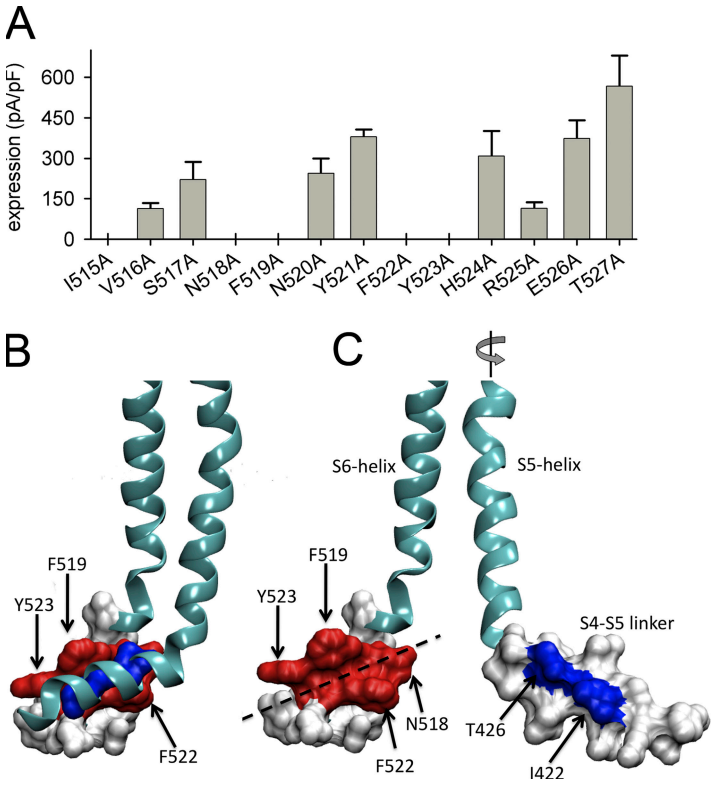

Figure 2. $S6_T$ is α-helical and forms a crevice that accommodates residues of L45. (A) Bar diagram showing the current level observed at +60 mV for the different alanine substitutions of $S6_T$. V516A and R522A displayed moderate expression, whereas others like I515A did not display any current at all. The periodicity of residues that tolerated a substitution or not is in favor of $S6_T$ adopting an α-helix. (B) hKv1.5 homology model (obtained as explained in Materials and methods) showing the S4-S5 linker and the S5 and S6 segments of one subunit. The positions in the $S6_T$ region that tolerated an alanine substitution are shown in gray space fill, whereas the residues that did not tolerate this substitution are in red. (C) The same view as in B, but with the L45 and S5 helix rotated (∼180°) away from the S6 segment to show both interacting surfaces. Note that the $S6_T$ residues that did not tolerate a substitution (red space fill) form a crevice in which residues of the S4-S5 linker fit. This crevice, highlighted with the dotted line, is largely created by the aromatic residues F519, F522, and Y523. For comparison, L45 is also shown in space fill with residues I422 and T426 (that likely reside in the $S6_T$ crevice) in blue.

were tested. hKv1.5 and hKv2.1 subunits do not form heterotetramers, and we hypothesized that if the L45 of hKv2.1 is not compatible with a hKv1.5 background, the channel would be nonfunctional. Therefore, the L45 linker was replaced in hKv1.5 (residues 418–432) by hKv2.1 sequence. As expected, the Kv1.5 chimera with an exchanged L45 (L45Kv2.1inKv1.5) did not generate currents within the voltage range of −130 to +130 mV (Fig. 3). Confocal imaging in combination with the immunocytochemistry approach as above showed that the chimera was retained intracellularly (Fig. S1, available at http://www.jgp.org/cgi/content/full/jgp.200810048/DC1). To narrow down the critical region in L45, we substituted nonconserved residues back to their hKv1.5 counterpart. This gradually back mutation approach in L45 (Table II) showed that mutating T418 back to a lysine (L45mutant1) and S422 back to an isoleucine (L45mutant2) was not sufficient to restore channel expression. Further replacing F425 for a lysine (L45mutant3) resulted in functional channels that activated slightly slower compared with WT hKv1.5 (Table II). Also, restoring hKv2.1 to hKv1.5 sequence at positions 431 and 432 (L45mutant4) resulted in functional channels that displayed a voltage dependence of activation that was shifted +25 mV toward positive voltages and with deactivation kinetics that were approximately five times faster than WT (Table II). Testing various combinations of back mutations to hKv1.5 sequence highlighted the double mutation K425F+R432N as most critical (Table II). This double mutation did express, but at very low levels, whereas mutants that changed only K425 or R432 to their hKv2.1 counterpart generated reasonable currents. The K425F+R432N mutant channels displayed a voltage dependence of activation that was shifted about +15 mV toward positive potentials with activation kinetics similar to WT hKv1.5.

As L45 of hKv2.1 was not compatible in an hKv1.5 background, we tested whether the additional replacement of the $S6_T$ region (residues 512–531) by corresponding hKv2.1 sequence might restore channel expression. Indeed, this double chimera L45S6Kv2.1inKv1.5 resulted in channels with a voltage dependence like hKv1.5 but with activation and deactivation kinetics comparable to hKv2.1 (Fig. 3 and Table II). This suggests that during and/or after folding, the $S6_T$ region of hKv2.1 adopts a different conformation than the one of hKv1.5, such that the necessary contacts with the L45 linker from hKv2.1 can be formed. Apparently, exchanging in hKv1.5 both L45 and $S6_T$ had no impact on the energy difference between both the closed and open state (similar midpoint) but altered the barrier between both states (reflected by the slower hKv2.1-type kinetics). Substituting only $S6_T$ in hKv1.5 by hKv2.1 sequence (S6Kv2.1inKv1.5) was unexpectedly tolerated. This chimera, S6Kv2.1inKv1.5,

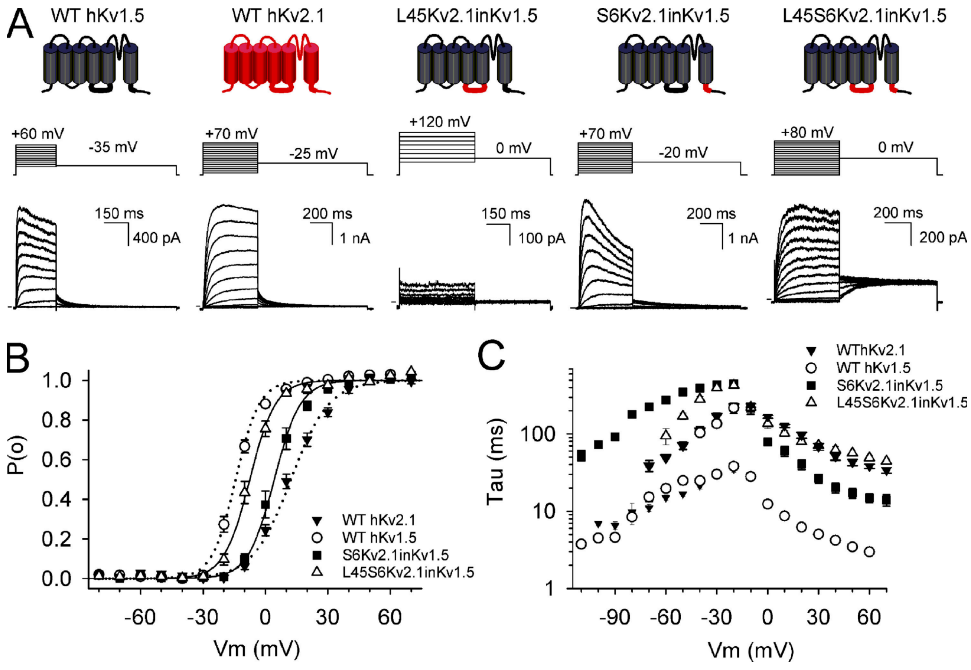

Figure 3. Properties of WT hKv1.5, WT hKv2.1, and chimeric constructs. (A) On top, a schematic representation for WT hKv1.5 (black subunit), WT hKv2.1 (red subunit), and the chimeric constructs is shown. In an hKv1.5 background, the S4-S5 linker (L45Kv2.1inKv1.5) or C-terminal S6 part (S6Kv2.1inKv1.5) was substituted by its corresponding counterpart of hKv2.1, indicated in red. On the bottom, the applied voltage protocols with corresponding K^+ currents are shown. Note that L45Kv2.1inKv1.5 was nonfunctional and that the expression could also be restored by replacing the C-terminal S6 part (L45S6Kv2.1inKv1.5). (B) Voltage dependence of activation obtained by plotting the normalized tail currents from A as a function of the applied voltage. (C) Both activation and deactivation time constants are represented. The activation kinetics of L45S6Kv2.1inKv1.5 resembled those of hKv2.1. The deactivation time constants of the chimeras were clearly slower than both WT channels.

TABLE II

Biophysical Properties of hKv2.1/hKv1.5 Chimeric Constructs

	S4-S5 linker							S6																													
hKv1.5	K	G	L	Q	I	L	G	K	T	L	Q	A	S	M	R	//	P	V	P	V	I	V	S	N	F	N	Y	F	Y	H	R	E	T	D	H	E	E
hKv2.1	**T**	–	–	–	**S**	–	–	**F**	–	–	**R**	**R**	–	**Y**	**N**	//	–	**I**	–	**I**	–	–	**N**	–	–	**S**	**E**	–	–	**K**	**E**	**Q**	**K**	**R**	**Q**	–	**K**
L45Kv2.1inKv1.5	**T**	–	–	–	**S**	–	–	**F**	–	–	**R**	**R**	–	**Y**	**N**	//	–	–	–	–	–	–	–	–	–	–	–	–	–	–	–	–	–	–	–	–	–
L45mutant1	–	–	–	–	**S**	–	–	**F**	–	–	**R**	**R**	–	**Y**	**N**	//	–	–	–	–	–	–	–	–	–	–	–	–	–	–	–	–	–	–	–	–	–
L45mutant2	–	–	–	–	–	–	–	**F**	–	–	**R**	**R**	–	**Y**	**N**	//	–	–	–	–	–	–	–	–	–	–	–	–	–	–	–	–	–	–	–	–	–
L45mutant3	–	–	–	–	–	–	–	–	–	–	**R**	**R**	–	**Y**	**N**	//	–	–	–	–	–	–	–	–	–	–	–	–	–	–	–	–	–	–	–	–	–
L45mutant4	–	–	–	–	–	–	–	**F**	–	–	**R**	**R**	–	–	–	//	–	–	–	–	–	–	–	–	–	–	–	–	–	–	–	–	–	–	–	–	–
L45mutant5	–	–	–	–	–	–	–	–	–	–	**R**	**R**	–	–	–	//	–	–	–	–	–	–	–	–	–	–	–	–	–	–	–	–	–	–	–	–	–
K425F+R432N	–	–	–	–	–	–	–	**F**	–	–	–	–	–	–	**N**	//	–	–	–	–	–	–	–	–	–	–	–	–	–	–	–	–	–	–	–	–	–
L45S6Kv2.1inKv1.5	**T**	–	–	–	**S**	–	–	**F**	–	–	**R**	**R**	–	**Y**	**N**	//	–	**I**	–	**I**	–	–	**N**	–	–	**S**	**E**	–	–	**K**	**E**	**Q**	**K**	**R**	**Q**	–	**K**
S6Kv2.1inKv1.5	–	–	–	–	–	–	–	–	–	–	–	–	–	–	–	//	–	**I**	–	**I**	–	–	**N**	–	–	**S**	**E**	–	–	**K**	**E**	**Q**	**K**	**R**	**Q**	–	**K**
Kv1.5chimera1	**T**	–	–	–	**S**	–	–	**F**	–	–	**R**	**R**	–	**Y**	**N**	//	–	**I**	–	**I**	–	–	**N**	–	–	**S**	**E**	–	–	–	–	–	–	–	–	–	–
Kv1.5chimera2	**T**	–	–	–	**S**	–	–	**F**	–	–	**R**	**R**	–	**Y**	**N**	//	–	–	–	–	–	–	**N**	–	–	**S**	**E**	–	–	**K**	**E**	**Q**	**K**	**R**	**Q**	–	**K**
Kv1.5chimera3	**T**	–	–	–	**S**	–	–	**F**	–	–	**R**	**R**	–	**Y**	**N**	//	–	**I**	–	**I**	–	–	–	–	–	–	–	–	–	**K**	**E**	**Q**	**K**	**R**	**Q**	–	**K**
Kv1.5chimera4	**T**	–	–	–	**S**	–	–	**F**	–	–	**R**	**R**	–	**Y**	**N**	//	–	–	–	**I**	–	–	–	–	–	–	–	–	–	**K**	**E**	**Q**	**K**	**R**	**Q**	–	**K**
Kv1.5chimera5	**T**	–	–	–	**S**	–	–	**F**	–	–	**R**	**R**	–	**Y**	**N**	//	–	–	–	**I**	–	–	–	–	–	–	–	–	–	–	–	**Q**	**K**	**R**	**Q**	–	**K**
Kv1.5chimera6	**T**	–	–	–	**S**	–	–	**F**	–	–	**R**	**R**	–	**Y**	**N**	//	–	–	–	**I**	–	–	–	–	–	–	–	–	–	–	–	**Q**	**K**	**R**	–	–	–
Kv1.5chimera7	**T**	–	–	–	**S**	–	–	**F**	–	–	**R**	**R**	–	**Y**	**N**	//	–	–	–	**I**	–	–	–	–	–	–	–	–	–	–	–	–	**K**	**R**	–	–	–
Kv1.5chimera8	**T**	–	–	–	**S**	–	–	**F**	–	–	**R**	**R**	–	**Y**	**N**	//	–	–	–	**I**	–	–	–	–	–	–	–	–	–	–	–	**Q**	**K**	–	–	–	–
Kv1.5chimera9	–	–	–	–	–	–	–	**F**	–	–	–	–	–	–	**N**	//	–	**I**	–	**I**	–	–	**N**	–	–	**S**	**E**	–	–	**K**	**E**	**Q**	**K**	**R**	**Q**	–	**K**
Kv1.5chimera10	–	–	–	–	–	–	–	**F**	–	–	–	–	–	–	**N**	//	–	–	–	**I**	–	–	–	–	–	–	–	–	–	–	–	**Q**	**K**	**R**	–	–	–

	I	$V_{1/2}$ (mV)	k (mV)	τ_a (ms)	τ_d (ms)	*n*	$V_{1/2,i}$ (mV)	k_i (mV)	*n*
hKv1.5	++	−14.3 ± 1.0	5.8 ± 0.2	3.5 ± 0.2	24.9 ± 2.5	9	−23.2 ± 1.3	3.9 ± 0.1	8
hKv2.1	++	12.3 ± 1.4	9.5 ± 0.6	33.8 ± 2.9	29.2 ± 2.2/170 ± 18	9	−15.9 ± 1.2	7.2 ± 0.6	5
L45Kv2.1inKv1.5	−								
L45mutant1	−								
L45mutant2	−								
L45mutant3	+	−20.6 ± 1.6	7.1 ± 0.2	10.1 ± 1.2	20.9 ± 3.2	7	−30.6 ± 1.1	4.1 ± 0.1	6
L45mutant4	+	11.1 ± 3.8	9.6 ± 1.0	3.9 ± 0.4	4.5 ± 0.9	6	−5.8 ± 1.6	5.0 ± 0.7	6
L45mutant5	+	−8.7 ± 2.4	9.8 ± 0.8	3.9 ± 0.2	2.0 ± 0.3	9	−16.9 ± 1.8	6.4 ± 0.4	8
K425F+R432N	+/−	0.8 ± 2.9	7.0 ± 0.8	4.7 ± 0.4	ND	3	ND	ND	
L45S6Kv2.1inKv1.5	+	−8.4 ± 1.4	6.2 ± 0.2	48.1 ± 3.3	170 ± 17	5	−18.4 ± 1.2	4.1 ± 0.4	3
S6Kv2.1inKv1.5	++	1.1 ± 2.5	6.0 ± 0.5	14.9 ± 2.0	395 ± 35	8	−8.7 ± 2.4	4.9 ± 0.3	5
Kv1.5chimera1	−								
Kv1.5chimera2	−								
Kv1.5chimera3	+	−13.9 ± 1.1	7.4 ± 0.4	39.9 ± 4.2	234 ± 40	7	−27.5 ± 0.6	5.4 ± 0.1	4
Kv1.5chimera4	+	−23.7 ± 2.3	6.0 ± 0.4	13.0 ± 1.4	513 ± 41	5	−37.1 ± 3.0	4.2 ± 0.6	4
Kv1.5chimera5	+	−31.3 ± 1.5	5.7 ± 0.6	10.6 ± 1.0	356 ± 52	6	−44.9 ± 1.3	4.8 ± 0.4	5
Kv1.5chimera6	+	−16.4 ± 1.4	7.3 ± 0.3	10.0 ± 0.9	306 ± 13	6	−31.2 ± 2.0	4.5 ± 0.4	5
Kv1.5chimera7	−								
Kv1.5chimera8	−								
Kv1.5chimera9	++	0.1 ± 1.3	6.0 ± 0.4	8.3 ± 0.9	366 ± 48	6	−11.8 ± 1.2	5.4 ± 0.4	5
Kv1.5chimera10	++	−12.4 ± 0.6	6.5 ± 0.3	4.6 ± 0.4	211 ± 18	9	−27.0 ± 0.6	4.0 ± 0.2	9

The L45 and $S6_T$ sequence of hKv1.5 is shown on top, above the hKv2.1 sequence. Mutant constructs were created in an hKv1.5 background with the respective substitutions set in bold. A + or − in column I indicates the presence or absence of time-dependent ionic current in the voltage range of −130 to +130 mV. The amount of plus signs represents the amplitude of K^+ current recorded. For the double mutant K425F+R432N, +/− indicates that only very small time-dependent currents were observed with a maximal current amplitude of ~50 pA with 7 µg cDNA transfected. $V_{1/2}$, k, and time constants τ_a at $V_{1/2}$ +60 mV and τ_d at $V_{1/2}$ −40 mV were obtained as in Table I. ND, not determined.

generated channels with a voltage dependence of activation that shifted +15 mV positive compared with WT hKv1.5. The time constants of activation were intermediate between those of hKv1.5 and hKv2.1, but channel closure was clearly impeded, as time constants were markedly slowed compared with both WT channels (Table II).

To investigate which residues of the $S6_T$ were responsible for rescue, the nonconserved residues were mutated back to hKv1.5 sequence. As was the case for L45,

this approach did not identify a unique residue that resulted in full rescue (Table II). However, we identified a combination of two molecular determinants that were important for restoring channel functionality (Table II). One was a single valine to isoleucine mutation (V514I) directly following the PXP motif, and the other was a cluster of three residues located further downstream replacing ETD by QKR. This Kv1.5chimera6 resulted in a channel with a voltage dependence of activation like hKv1.5 (Fig. 4). Compared with hKv2.1 and the chimera L45S6Kv2.1inKv1.5, the activation time constants were approximately four times faster, but deactivation remained as slow (Fig. 4). Furthermore, in the double L45 mutant K425F+R432N, channel expression was also restored by replacing the complete $S6_T$ region by hKv2.1 sequence or by only the two most crucial determinants (Fig. 4 and Table II).

The residues identified by the alanine/glycine substitution scan as important in $S6_T$ were fully conserved between hKv1.5 and hKv2.1 (Tables I and II). This suggests that the $S6_T$ in both hKv1.5 and hKv2.1 adopt a similar "crevice" structure, and that a different orientation of the $S6_T$ and L45 regions makes the latter one not interchangeable. The most obvious differences between hKv1.5 and hKv2.1 were the neutralization of the positive charges K425 and R432 in L45 and the EDT to QKR charge reversal in $S6_T$. To test for possible electrostatic interactions, both K425 and R432 in hKv1.5 were mutated into the negatively charged aspartate. Surprisingly, both mutants (K425E and R432E) resulted in channels that expressed well and had biophysical properties similar to WT hKv1.5. Apparently, the distortion of the local electric field at these positions in L45 did not impede channel functionality. To further investigate the role of these residues, we mutated both residues one by one to their corresponding hKv2.1 counterpart. The K425F mutation in hKv1.5 reduced channel expression drastically; as a result, the deactivation kinetics could not be determined adequately, but the voltage dependence and kinetics of activation were comparable to WT. An alanine substitution (K425A) also reduced channel expression but shifted the voltage dependence of activation and inactivation with +25 mV toward positive potentials. Substituting the positively charged arginine at position 432 by the corresponding hKv2.1 asparagine (R432N) also shifted the voltage dependence toward positive potentials and slowed down deactivation by twofold. Replacing R432 by a phenylalanine (which is more hydrophobic than an asparagine) shifted the voltage dependence of activation and inactivation even more positive, ~+30 mV compared with WT. These results indicate that it was not the charge neutralization in L45 but the change in overall hydrophobicity that distorted channel function.

To test if hydrophobicity is a major determinant for the conformation of L45 and $S6_T$, the mean hydrophobic vector of both regions was calculated. Given that $S6_T$ and probably L45 is α-helical, the mean hydrophobic vector was calculated as described by Eisenberg et al., (1982) using the assumption of an α-helical pattern and the scaled hydrophobicities for each residue as determined by Black and Mould (1991). For these calculations, we used windows with boundaries that included or excluded the crucial residues. For L45 the complete

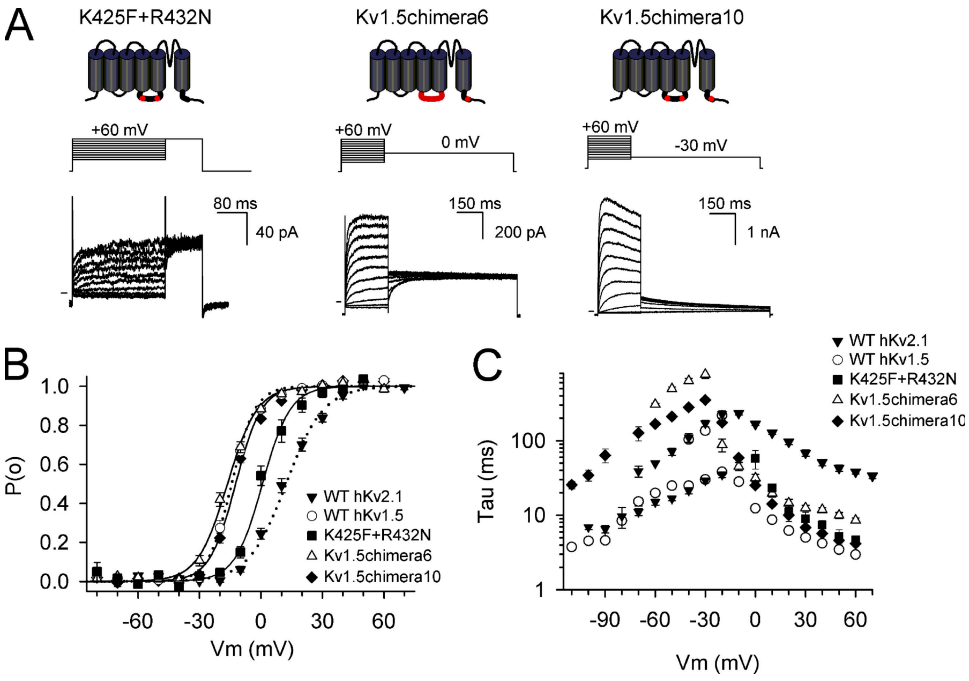

Figure 4. Properties of K425F+R432N, Kv1.5chimera6, and Kv1.5chimera10. (A) On top, a schematic representation of the double mutant K425F+R432N and the Kv1.5chimera6 containing the most critical residues of the $S6_T$ region is shown. Kv1.5chimera10 contains only the critical residues in both L45 and $S6_T$. (B) Both chimeras had a voltage dependence of activation like WT hKv1.5 and the chimera L45S6Kv2.1inKv1.5. (C) Chimera 10 displayed a slowing of deactivation similar to L45S6Kv2.1inKv1.5 but activated much faster, resembling WT hKv1.5 activation. On the other hand, chimera 6 displayed gating kinetics similar to L45S6Kv2.1inKv1.5. This indicated that regarded to chimera 10, chimera 6 contained residues in L45 that slowed activation compared with WT hKv1.5.

region was used, which in hKv1.5 ranged from residue L418 to R432. For hKv2.1 and the mutant constructs, the corresponding residue window was used. The resulting hydrophobic vectors displayed a clear difference in orientation between hKv1.5 or hKv2.1 sequence (Fig. 5). The mean hydrophobic vector of L45 from the double mutant K425F+R432N tended toward that of hKv2.1, consistent with this double mutation in L45 being most critical. To determine the effect of changes in the hydrophobic vector of $S6_T$, we used a window section that excluded the region that constitutes the crevice, as the high sequence homology caused an overlap in hydrophobic moment between hKv1.5 and hKv2.1 if included. Therefore, the window used for $S6_T$ ranged in hKv1.5 from H524 to E530. Because L45 is amphipathic (or amphiphilic), the mean hydrophobic vectors obtained for this segment were larger than the ones for $S6_T$. Using this window for $S6_T$, the difference in hydrophobic vector between hKv1.5 and hKv2.1 matched the difference observed for L45 (Fig. 5). The hydrophobic vector of $S6_T$ for the Kv1.5chimera10 tended toward those of hKv2.1, whereas the one of Kv1.5chimera7, which did not result in rescue, overlaps with the one of hKv1.5 (Fig. 5).

Replacing Residues in L45 and $S6_T$ of hKv1.5 by Their hKv2.1 Counterpart

To determine the effect of the other nonconserved residues in L45, all residues that differed between hKv1.5 and hKv2.1 were individually replaced in an hKv1.5 background. The mutations K418T, Q428R, and M431F were well tolerated and resulted in channels with biophysical properties similar to WT hKv1.5 (Table III). On the other hand, at position A429 the substitution by an arginine (A429R) generated a channel with a voltage dependence like WT but with deactivation time constants that were approximately five times faster. Furthermore, the mutant I422S resulted in channels that displayed markedly perturbed gating. Besides a −10-mV shift in their voltage dependence, the activation kinetics were slowed by fourfold and channel deactivation was slowed by 20-fold. On an α-helical wheel representation, residues A429 and I422 cluster apparently more or less on the same side as residues K425 and R432, which impeded channel expression upon substitution by hydrophobic residues. On the other hand, both Q428 and M431 cluster at the opposite side in L45, presumably one which is less critical (Fig. 5).

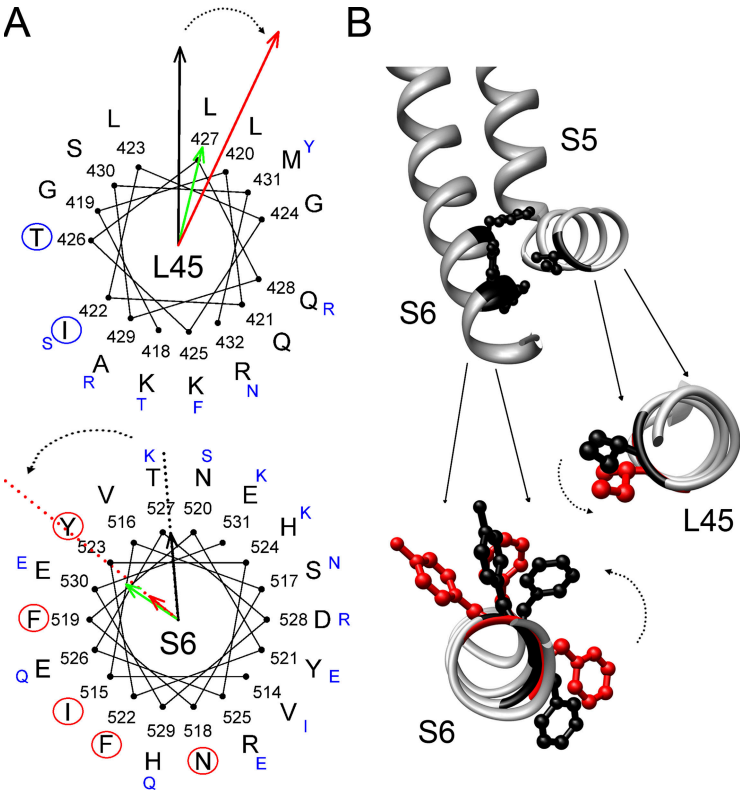

Figure 5. α-helical wheel representation with hydrophobic vector for both L45 and $S6_T$. (A, top) The L45 residues K418 to R432, with hKv1.5 sequence in boldface and small uppercase blue letters indicating different residues found in hKv2.1. The hydrophobic vectors for hKv1.5 and hKv2.1 are indicated with a black and a red arrow, respectively. The hydrophobic vector of the double mutant K425F+R432N is shown in green. The residues that most likely reside in the $S6_T$ crevice are encircled in blue. (Bottom) The $S6_T$ residues V514 to E531 of hKv1.5, with hydrophobic vectors color coded as in the top. Residues that are conserved between hKv1.5 and hKv2.1 did not tolerate an alanine substitution in hKv1.5 (red encircled). Similar to the representation of L45 above, the hydrophobic vector of hKv1.5 is shown in black, whereas the one of hKv2.1 is shown in red. In green, the hydrophobic vector of the rescue Kv1.5chimera5 is shown. Note the relative rotation between the vectors of hKv1.5 and hKv2.1 (for both L45 and $S6_T$). (B) The possible structural repercussion of the swiveled hydrophobic vector. For the WT hKv1.5 situation, we used our generated homology model (see Materials and methods). On top, a representation of the coupling between L45 and $S6_T$ in WT hKv1.5 with residue I422 of the L45 and residues F519, F522, and Y523 on S6 in black is shown. On the bottom, close ups of the L45 and bottom part of S6 that show the effect of swiveling both segments in such a way that the hydrophobic vectors of hKv1.5 and hKv2.1 (shown in A) match each other are shown. When the L45 is swiveled ∼20°, residue I422 would orient more toward the cytoplasm (in the representation downward). The position of residue I422 in a WT hKv1.5 situation is colored black. If the swivel of the hydrophobic vector reorients the L45, residue I422 would occupy the (hypothetical) position indicated in red. The effect of swiveling $S6_T$ according to the difference in hydrophobic vector is represented below, again with the position of residues F519, F522, and Y523 in WT hKv1.5 indicated in black and the hypothetical position after swiveling shown in red. The direction of the rotation between WT and chimeric constructs is indicated in all panels with a dotted arrow.

TABLE III

Biophysical Properties of Individual Substitutions in hKv1.5

hKv1.5	K	G	L	Q	I	L	G	K	T	L	Q	A	S	M	R	E	
	I		I		I		I		I		I		I		I		
position	418		420		422		424		426		428		430		432		
	(380)		(382)		(384)		(386)		(388)		(390)		(392)		(392)		
					Activation						Deactivation				Inactivation		
	$V_{1/2}$ (mV)		k (mV)		τ_a (ms)				τ_d (ms)				$V_{1/2,i}$ (mV)		k_i (mV)		*n*
K418T	1.5 ± 1.5		7.3 ± 0.6		4.5 ± 0.4				22.8 ± 3.0				−8.2 ± 0.7		4.9 ± 0.3		6
I422S	−26.4 ± 1.9		6.9 ± 0.6		12.6 ± 0.9				475 ± 27				−38.9 ± 1.0		4.5 ± 0.2		5
I422A	−24.1 ± 2.3		7.0 ± 0.7		5.7 ± 0.4				277 ± 52				−33.7 ± 1.7		5.8 ± 0.3		7
I422W	no current																
I422R	no current																
K425E	−10.1 ± 1.9		6.0 ± 0.3		4.3 ± 0.3				18.9 ± 3.2				−16.4 ± 1.4		3.6 ± 0.3		5
K425F	−5.2 ± 2.7		6.2 ± 1.3		7.8 ± 1.0				ND				ND		ND		3
K425A	12.2 ± 1.6		7.0 ± 0.3		5.7 ± 0.8				19.2 ± 1.9				2.9 ± 1.5		5.5 ± 0.3		6
T426A	−1.5 ± 2.0		6.6 ± 0.3		3.6 ± 0.2				6.6 ± 0.8				−13.9 ± 2.6		4.5 ± 0.4		5
T426W	no current																
T426R	no current																
Q428R	−9.7 ± 1.4		6.5 ± 0.2		5.0 ± 0.8				22.0 ± 5.2				−19.3 ± 0.6		5.0 ± 0.1		5
A429R	−8.2 ± 1.8		7.1 ± 0.5		7.0 ± 0.6				4.4 ± 0.5				−16.2 ± 2.6		5.2 ± 0.3		5
M431F	−11.1 ± 1.4		5.9 ± 0.3		5.5 ± 0.9				16.1 ± 1.4				−16.3 ± 0.9		4.9 ± 0.3		6
R432E	−9.4 ± 0.6		4.9 ± 0.3		3.0 ± 0.3				13.7 ± 0.3				−14.0 ± 1.5		4.1 ± 0.2		4
R432N	−1.6 ± 1.2		5.8 ± 0.2		4.4 ± 0.5				57.0 ± 5.3				−7.5 ± 1.4		4.5 ± 0.2		8
R432F	17.4 ± 1.3		7.0 ± 0.5		5.9 ± 0.7				12.5 ± 0.5				2.0 ± 1.1		4.3 ± 0.3		7
V514I	−5.1 ± 1.7		5.4 ± 0.7		4.5 ± 0.5				223 ± 19				−12.4 ± 1.4		3.6 ± 0.3		5
Y521E	−14.9 ± 1.4		5.3 ± 0.4		3.5 ± 0.3				11.9 ± 1.1				−22.8 ± 2.1		3.7 ± 0.4		5
H524K	−5.0 ± 1.6		4.6 ± 0.4		4.0 ± 0.4				26.6 ± 2.7				−11.5 ± 1.3		4.0 ± 0.1		5
R525E	−16.5 ± 0.9		5.6 ± 0.4		3.5 ± 0.2				25.8 ± 2.1				−26.4 ± 0.9		3.2 ± 0.1		6
E526Q	−9.6 ± 0.3		5.1 ± 0.3		4.8 ± 0.6				13.8 ± 1.8				−16.8 ± 1.2		4.5 ± 0.2		4
T527K	−7.1 ± 0.3		5.1 ± 0.2		4.2 ± 0.5				17.9 ± 3.2				−12.3 ± 1.4		3.8 ± 0.3		5
D528R	−10.9 ± 1.5		5.3 ± 0.5		4.7 ± 0.4				26.6 ± 2.6				−18.4 ± 0.6		4.0 ± 0.2		7
H529Q	−3.7 ± 1.2		5.0 ± 0.4		4.2 ± 0.5				18.8 ± 2.3				−9.0 ± 2.0		4.1 ± 0.4		6
E531K	−9.9 ± 2.8		5.6 ± 0.6		4.9 ± 0.5				20.4 ± 1.6				−17.0 ± 1.1		3.5 ± 0.2		5

Sequence of L45 from hKv1.5 on top with *Shaker* numbering between parentheses. All mutations were done in an hKv1.5 background, and $V_{1/2}$, k, and t were obtained as in Table I. ND, not determined.

According to the 3-D crystal structure of rKv1.2, residue I422, whose substitution affected gating most profoundly, is in close contact with the bottom part of S6. Likewise, residue T426, which is conserved between hKv1.5 and hKv2.1, is likely to make contact. To check the latter possibility, both residues were further mutated in a tryptophan (a bulky residue to perturb protein contacts), an alanine (small side chain and losing potential interactions), and an arginine that is charged and highly hydrophilic. At both positions neither a tryptophan nor arginine was tolerated. An alanine substitution was tolerated but altered channel gating markedly. I422A displayed a negatively shifted voltage dependence of activation and slowed down deactivation by 10-fold, similar to I422S (Table III and Fig. S2, which is available at http://www.jgp.org/cgi/content/full/jgp.200810048/DC1). On the other hand, an alanine substitution for T426 shifted the voltage dependence of activation with +10 mV more positive and displayed fivefold faster deactivation time constants compared with WT (Table III and Fig. S2). In both cases the activation time constants were similar to WT. This indicated that I422A stabilized the open state, whereas T426A did the opposite. As expected from our alanine/glycine substitution scan of $S6_T$, the individual substitution of the residues that differed between hKv1.5 and hKv2.1 did not identify residues that were individually critical for channel gating. A noted exception was position 514, where the conservative substitution of a valine by an isoleucine (V514I) slowed down channel closure drastically compared with WT and might explain the impaired channel closure of several of the chimeras that contained this V514I mutation. This indicates that this residue is involved in the gating process and is in agreement with the observation that this V514I mutation is needed for making the L45 of hKv2.1 compatible in an hKv1.5 background (Table II). In conclusion, the one by one substitution in hKv1.5 of residues that differed from hKv2.1 did not uncover a

unique single pair of L45/$S6_T$ residues (Tables II and III) that was responsible for the distortion or rescue of channel gating, indicating that multiple residues determine the proper contact.

DISCUSSION

The α-helical Configuration of $S6_T$ Is Essential for Gating of Kv Channels

Individual glycine and alanine substitution of residues 515–527 in hKv1.5 resulted in a periodicity for functional and nonfunctional channels every three to four residues, which supports an α-helical configuration for this region (Table I and Fig. 2). Furthermore, substitutions for proline residues, which destabilize an α-helical configuration because of the loss of an H bond, were not tolerated (O'Neil and DeGrado, 1990; Blaber et al., 1993). At position V516, an alanine substitution was tolerated but a glycine substitution was not, likely because this residue is a prime candidate to occlude the pore in the closed state (del Camino and Yellen, 2001; Hackos et al., 2002). The homologous V516G mutation in *Shaker* (V478G) was functional but resulted likewise in a channel that expressed poorly (Kitaguchi et al., 2004). Because a cysteine substitution at this position (V478C) was able to react with methanethiosulfonate reagents and was sensitive to cadmium block (Liu et al., 1997; del Camino and Yellen, 2001), this residue must be accessible from the cytosol and should thus be facing the ion-conducting pore. Because both the crystal structure and our functional results favor an α-helical structure for the $S6_T$ region, the subsequent residues S517, N520, Y521, H524, and R525 are most likely also exposed (Fig. 2). The observation that S517 can be replaced by a glutamate that is negatively charged further supports its orientation toward the pore or at least an aqueous environment (Yeola et al., 1996).

The residues N518, F519, F522, and Y523 that did not tolerate a substitution map on the other side of the $S6_T$ α-helix (Fig. 5), which is therefore probably important for channel gating and/or channel folding (protein packing). These two possibilities are not necessarily mutually exclusive because the failure to fold properly could be due to the inability to create the contacts that are crucial for channel gating. Because neither glycine nor alanine substitutions were tolerated, the nonfunctionality is indeed likely due to the loss of required side chain interactions. Alanine and cysteine substitutions of N480 and F481 in *Shaker* (N518 and F519 in hKv1.5) also resulted in subunits that failed to express functional channels, whereas a tryptophan substitution at that position was well tolerated (Liu et al., 1997; Hackos et al., 2002). The homologous residues of F522 and Y523 in *Shaker* (F484 and Y485, respectively) were also critical for normal gating, indicating that these residues form part of the gating machinery (Ding and Horn, 2002; Hackos et al., 2002; Ding and Horn, 2003).

An hKv1.5 homology model based on the rKv1.2 structure (Long et al., 2005a) shows that the residues that are sensitive to substitutions orient toward L45, and that the individual substitution of residues N518, F519, F522, and Y523 to an alanine or glycine created a cavity (Fig. S3, available at http://www.jgp.org/cgi/content/full/jgp.200810048/DC1). The creation of such cavities could cause structural rearrangements as surrounding residues move toward the vacant space (Eriksson et al., 1992). If hydrogen bonds are present, replacing residues with bulkier side chains by alanines would result in unpaired hydrogen-bonding partners. Furthermore, water may penetrate into the cavity and form a hydrogen bond with the partner. Thus, mutations that create cavities are very destabilizing because of the loss of van der Waals interactions and possible hydrogen bonds. In this model, the aromatic side chains of residues F519, F522, and Y523 form a crevice, with the upper wall formed mainly by F519 and the bottom one by F522 (Fig. 2). Thus, the region on $S6_T$ that presumably couples to the L45 adopts a crevice in which residues from L45 can reside.

Coupling between L45 and $S6_T$ Requires a Correct Conformation of Both Regions

Substituting the L45 of hKv1.5 by the linker sequence of hKv2.1 resulted in nonfunctional channels that did not pass the ER quality control. Apparently, the opposite exchange was tolerated, as an hKv2.1 channel with the L45 sequence of Kv1.2 was functional (Scholle et al., 2004). Also, the L45 of *Shaw* and Kv3.4 channels was interchangeable (Bhattacharji et al., 2006). This suggests that subtle differences in sequence between Kv channels determine the mutual compatibility of L45. At first glance, the result of our L45 chimeras between hKv2.1 and hKv1.5 differs from the observation that heterotetramers between hKv2.1 and *Shaker* are possible after removing the N-terminal T1 domain (Li et al., 1992). However, our results indicate that the L45-$S6_T$ compatibility is based on intra-subunit interactions that are most likely maintained in the heteromeric channels (Labro et al., 2005; Long et al., 2005a).

To make the L45 of hKv2.1 compatible in an hKv1.5 background, it was sufficient to also replace $S6_T$ by the corresponding hKv2.1 sequence. This double chimera resulted in channels with a voltage dependence similar to that of hKv1.5 but with hKv2.1-like kinetics. The observed hKv1.5-type voltage dependence would thus result from the VSD that is still from hKv1.5. The hKv2.1-like kinetics suggest that the constraints on the movement of the electromechanical coupling have been changed, most likely reflecting those of hKv2.1. Thus, exchanging the "full coupling unit" can transfer hKv2.1 kinetics to a hKv1.5 background, which indicates

that differences in coupling constraints may determine the different gating kinetics observed throughout the Kv family.

Previous work suggested that the L45 is also α-helical (Ohlenschlager et al., 2002), and this was further indicated by the 3-D crystal structure of rKv1.2 (Long et al., 2005a). When the residues of both L45 and $S6_T$ were mapped on an α-helical wheel representation, the residues that differ between hKv1.5 and hKv2.1 cluster for both regions at one side of the helix (Fig. 5). However, in the hKv1.5 homology model, these regions of L45 and $S6_T$ are (unexpectedly) not in direct contact. Apparently, the critical residues in $S6_T$ that constitute the crevice and the residues of L45 that reside in it are conserved in both channels. Also, the leucine repeat in L45 is fully preserved. Substitutions of these leucine residues in *Shaker* affected the channel's biophysical properties probably because several of these leucine residues face the lipid bilayer (Isacoff et al., 1991; McCormack et al., 1991; Long et al., 2005a). The recent 3-D crystal structure of a Kv channel in a membrane-like environment indeed showed the presence of lipids in the vicinity of L45 (Long et al., 2007). Thus, the majority of residues that mutually differ between hKv1.5 and hKv2.1 map on the side of L45, which presumably faces the cytoplasm.

The individual substitution of residues K425 and R432 indicated that the impact of the substitution depended largely on the change in hydrophobicity. Because the reduction in entropy is an important determinant for protein folding, hydrophobicity of certain channel regions may be a critical regulator and changes in overall hydrophobicity might cause regions to orient differently. The orientation of the hydrophobic vector of L45 indeed differed between hKv1.5 and hKv2.1, and a rotation of ∼20° is needed to match both vectors. These different vector orientations may explain why the L45 of hKv2.1 is incompatible in an hKv1.5 background, whereas the opposite is tolerated. Similar to L45, the mean hydrophobic vector of the lower part of $S6_T$ differs between hKv1.5 and hKv2.1 by a rotation of ∼20°. Thus, simultaneously changing the orientation of both $S6_T$ and L45 results in a configuration in which the residues that constitute the L45/$S6_T$ coupling come in close proximity again (Fig. 5 B). However, another crucial determinant for rescue was the EDT to QKR charge reversal in $S6_T$, and we cannot exclude that this charge cluster interacts with channel parts other than L45 and thereby positions $S6_T$. Thus, several residues in both L45 and $S6_T$ that are supposedly not making the coupling contacts themselves are needed to orient both

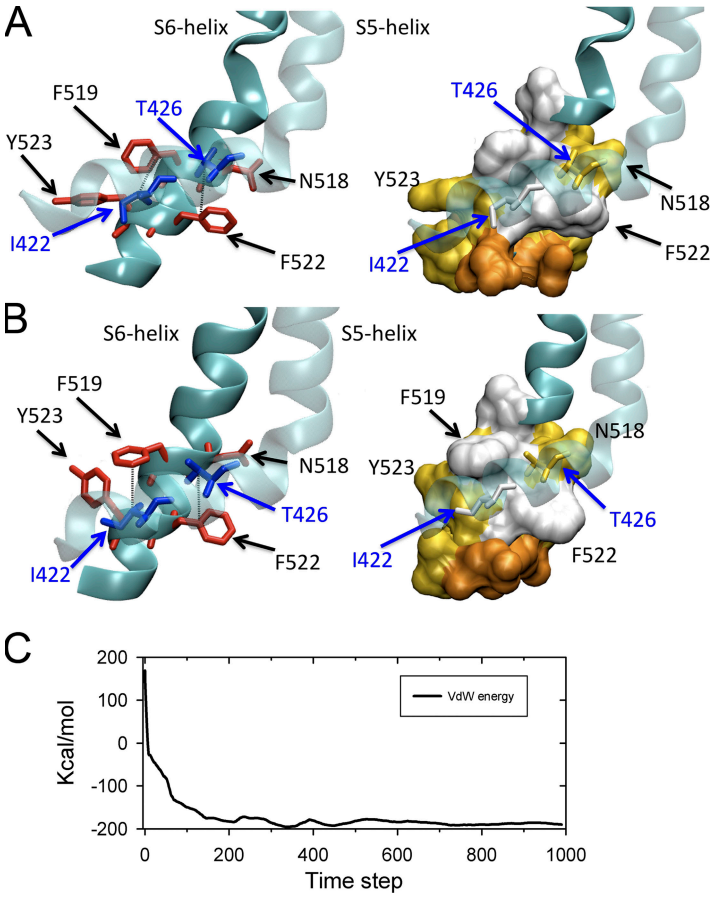

Figure 6. Structural model of the mechanical coupling. (A) Side view of the coupling between L45 and $S6_T$ region in the hKv1.5 homology model. The L45 and S5 segment are displayed in transparence to show the interaction between residues. On the left, the important residues I422 and T426 of L45 are shown in blue. The residues that form the crevice in $S6_T$ are shown in red. In this model, the residue I422 of L45 is positioned beneath residue F519 of the $S6_T$, whereas residue T426 is positioned above residue F522. On the right, the same point of view is shown but with color coding according to the hydrophobicity of the residues. White refers to hydrophobic residues, whereas an increased orange tone reflects an increase in the hydrophilic nature of the residue. Note that the $S6_T$ crevice is largely hydrophobic. (B) Similar views on the mechanical coupling as in panel A, but in this case a hypothetical model was used (instead of the hKv1.5 homology model) that was obtained and optimized as described in Materials and methods. In this model, the L45 is reoriented such that I422 and T426 come closer to their respective interacting residues F519 and F522. The distance between both pairs is indicated with a dotted line in the representation on the left. (C) Van der Waals energy shown as a function of the MD time step during optimization of our hypothetical model. The graph shows the nonbonding Van der Waals energy of the total potential energy that was defined by the CHARMM19 force field (see Materials and methods). The initial value (step 1) refers to the starting energy of the distorted model in which L45 was manually positioned such that residues I422 and T426 came within contact distance to F519 and F522, respectively. The last value (step 1,000) corresponds to the optimized model that is shown in B. The plot clearly shows the drop of Van der Waals energy and indicates that a local energy minimum is reached, which is compatible with an optimized new position of the L45 with respect to $S6_T$.

regions correctly and maintain the correct structure of the coupling. Consequently, an incorrect conformation might result in an incomplete coupling with altered kinetics or even misfolded channels.

Motions at the Contact Interface between S4-S5 Linker and $S6_T$

The movement of the VSD is most likely translated in opening and/or closing of the channel gate through L45, which works as a lever that exerts force on $S6_T$. The exact motions at these contacts have not yet been resolved. Although it is not straightforward to interpret changes in gating functions from mutations, the combination of our biophysical results with the constructed models indicate that multiple residue contacts are important in the electromechanical coupling, and that they can be divided in at least two groups: those residues that effectively transduce the mechanical energy, and others outside the interacting surface that are critical to maintain the correct 3-D configuration that allows and constrains the interaction ("contact residues" vs. "structural residues"). This might be compared with the structures for the mechanical interaction and stability of a ball and socket joint (e.g., hip joint): the cartilage forms the surface that transmits the mechanical energy, but the surrounding structure (ligaments and the rim of the socket) hold the two interacting faces in place. Thus, the interactions between the contact residues are not needed to keep the overall structure intact; therefore, the coupling contacts between both regions need not be very tight. This allows for both dynamic motions at the coupling interface and for the work to be exerted for the transition between the closed and open state. In the homology model, the side of L45 that resides in the $S6_T$ crevice contains residues I422 and T426. Because channel gating is a dynamic process, some of the contacts may only be transient, or only be present in either the open or closed conformation. Because the rKv1.2 channel structure was determined in an open configuration (Long et al., 2005a), it is possible that the side on L45 that forms the coupling is wider and residue A429 comes in close contact with the bottom part of S6 upon channel closure. This is supported by the observation that mutating this residue speeds up channel deactivation (Table III and Fig. S2). However, in the open state this residue should be exposed and accessible, as it is documented that the corresponding residue in *Shaker* (A391) forms part of the putative binding site for the inactivating N-ball (Holmgren et al., 1996). Thus, if residue A429 forms part of the coupling, L45 or $S6_T$ would rotate slightly during channel gating.

The individual substitution of residues I422 and T426 resulted in channels with markedly altered gating (Table III). The observed shifted voltage dependence of T426A is similar to the corresponding T388A mutant in *Shaker* (Isacoff et al., 1991). Initially, it was proposed that this T388 residue in *Shaker* contributed to the binding site for the inactivating N-ball, but this was later revised and the observed effects on inactivation upon mutation are most likely a reflection of their effect on the electromechanical coupling (Isacoff et al., 1991; Holmgren et al., 1996). Our results show that mutating I422 impaired channel closure, whereas the substitutions of T426 speeded up deactivation. Therefore, both residues apparently stabilize a different conformational state of the channel. The fact that both residues map on the same side of L45 is not in favor of significant rotational motions at the contact interface between L45 and $S6_T$. If both residues would occupy the $S6_T$ crevice alternately in the open- or closed-channel conformation, this would suggest a sliding motion of the residues through the contact interface (crevice). Alternatively, this could indicate that residues I422 and T426 act on different residues of the $S6_T$ crevice and alternately push on their contacts, depending on the gating transition (open-to-closed or closed-to-open).

Pathak et al. (2007) suggested in their recent model that to translate the VSD movement into gate opening, the N-terminal part of S5 needs to twist first. In this way, it unlocks the coupling before the $L45/S6_T$ could reorient. For the movement of L45 itself, they suggested a radial motion parallel to the lipid bilayer, preserving its location between the hydrophobic and polar layers of the membrane. Such a movement differs from the more downward movement of the N-terminal part of L45 proposed by Long et al. (2005b, 2007). The difference between both models is that the L45 linker pushes $S6_T$ mainly sideways in the former and downward in the latter. Despite this (slightly) different mechanism, significant rotational movements are absent in both. In Pathak's model, both I422 and T426 also reside in the $S6_T$ crevice, and their interaction site remains roughly the same in both the open and closed state. According to our hKv1.5 homology model, T426 might contact residue F522 and I422 residues F519 and Y523 (Fig. 6). We propose that these contacts are largely responsible for the mechanical coupling of the L45 with S6T, and that the type of interactions is mainly carried by Van der Waals interactions. This hypothesis is supported by the energy minimization of the speculative model of the L45/S6T coupling that evidenced the contribution of the Van der Waals interactions (Fig. 6 C).

Collectively, our results show that the α-helical configuration of S6 is required for the creation of a $S6_T$ crevice in which the L45 resides. The residues at the contact interface most likely make up the mechanical coupling, whereas the flanking residues serve a stabilizing and structural role by orienting L45 and $S6_T$ correctly.

We are grateful to J.P. Timmermans for the use of the confocal microscope and to T. de Block and T. Bruyns for their excellent technical assistance.

A.J. Labro is a postdoctoral fellow with the Fonds voor Wetenschappelijk Onderzoek Vlaanderen. This work was supported by grants from the Fonds voor Wetenschappelijk Onderzoek Vlaanderen (FWO-1.5.044.07, FWO-G.0152.06, FWO-G.0035.05, and FWO-G.0256.08), IAP6/31 of the Interuniversity Attraction Poles Program (Belgian State) Belgian Science and Policy, and a TOP08 project of the University of Antwerp.

Lawrence G. Palmer served as editor.

Submitted: 19 May 2008
Accepted: 30 October 2008

REFERENCES

Bezanilla, F. 2000. The voltage sensor in voltage-dependent ion channels. *Physiol. Rev.* 80:555–592.

Bhattacharji, A., B. Kaplan, T. Harris, X. Qu, M.W. Germann, and M. Covarrubias. 2006. The concerted contribution of the S4-S5 linker and the S6 segment to the modulation of a Kv channel by 1-alkanols. *Mol. Pharmacol.* 70:1542–1554.

Blaber, M., X.J. Zhang, and B.W. Matthews. 1993. Structural basis of amino acid alpha helix propensity. *Science.* 260:1637–1640.

Black, S.D., and D.R. Mould. 1991. Development of hydrophobicity parameters to analyze proteins which bear post- or cotranslational modifications. *Anal. Biochem.* 193:72–82.

Boussif, O., F. Lezoualc'h, M.A. Zanta, M.D. Mergny, D. Scherman, B. Demeneix, and J.P. Behr. 1995. A versatile vector for gene and oligonucleotide transfer into cells in culture and in vivo: polyethylenimine. *Proc. Natl. Acad. Sci. USA.* 92:7297–7301.

Caprini, M., M. Fava, P. Valente, G. Fernandez-Ballester, C. Rapisarda, S. Ferroni, and A. Ferrer-Montiel. 2005. Molecular compatibility of the channel gate and the N terminus of S5 segment for voltage-gated channel activity. *J. Biol. Chem.* 280:18253–18264.

Decher, N., J. Chen, and M.C. Sanguinetti. 2004. Voltage-dependent gating of hyperpolarization-activated, cyclic nucleotide-gated pacemaker channels: molecular coupling between the S4-S5 and C-linkers. *J. Biol. Chem.* 279:13859–13865.

del Camino, D., and G. Yellen. 2001. Tight steric closure at the intracellular activation gate of a voltage-gated K^+ channel. *Neuron.* 32:649–656.

Ding, S., and R. Horn. 2002. Tail end of the S6 segment: role in permeation in *Shaker* potassium channels. *J. Gen. Physiol.* 120:87–97.

Ding, S., and R. Horn. 2003. Effect of S6 tail mutations on charge movement in *Shaker* potassium channels. *Biophys. J.* 84:295–305.

Eisenberg, D., R.M. Weiss, and T.C. Terwilliger. 1982. The helical hydrophobic moment: a measure of the amphiphilicity of a helix. *Nature.* 299:371–374.

Eriksson, A.E., W.A. Baase, X.J. Zhang, D.W. Heinz, M. Blaber, E.P. Baldwin, and B.W. Matthews. 1992. Response of a protein structure to cavity-creating mutations and its relation to the hydrophobic effect. *Science.* 255:178–183.

Ferrer, T., J. Rupp, D.R. Piper, and M. Tristani-Firouzi. 2006. The S4-S5 linker directly couples voltage sensor movement to the activation gate in the human ether-a'-go-go-related gene (hERG) K^+ channel. *J. Biol. Chem.* 281:12858–12864.

Hackos, D.H., T.H. Chang, and K.J. Swartz. 2002. Scanning the intracellular S6 activation gate in the *Shaker* K^+ channel. *J. Gen. Physiol.* 119:521–532.

Holmgren, M., M.E. Jurman, and G. Yellen. 1996. N-type inactivation and the S4-S5 region of the *Shaker* K^+ channel. *J. Gen. Physiol.* 108:195–206.

Humphrey, W., A. Dalke, and K. Schulten. 1996. VMD: visual molecular dynamics. *J. Mol. Graph.* 14:33–38.

Isacoff, E.Y., Y.N. Jan, and L.Y. Jan. 1991. Putative receptor for the cytoplasmic inactivation gate in the *Shaker* K^+ channel. *Nature.* 353:86–90.

Kitaguchi, T., M. Sukhareva, and K.J. Swartz. 2004. Stabilizing the closed S6 gate in the *Shaker* Kv channel through modification of a hydrophobic seal. *J. Gen. Physiol.* 124:319–332.

Labro, A.J., A.L. Raes, and D.J. Snyders. 2005. Coupling of voltage sensing to channel opening reflects intrasubunit interactions in Kv channels. *J. Gen. Physiol.* 125:71–80.

Laskowski, R.A., M.W. MacArthur, D.S. Moss, and J.M. Thornton. 1993. Procheck—a program to check the stereochemical quality of protein structures. *J. Appl. Cryst.* 26:283–291.

Li, M., Y.N. Jan, and L.Y. Jan. 1992. Specification of subunit assembly by the hydrophilic amino-terminal domain of the *Shaker* potassium channel. *Science.* 257:1225–1230.

Liu, Y., M. Holmgren, M.E. Jurman, and G. Yellen. 1997. Gated access to the pore of a voltage-dependent K^+ channel. *Neuron.* 19:175–184.

Long, S.B., E.B. Campbell, and R. MacKinnon. 2005a. Crystal structure of a mammalian voltage-dependent *Shaker* family K^+ channel. *Science.* 309:897–903.

Long, S.B., E.B. Campbell, and R. MacKinnon. 2005b. Voltage sensor of Kv1.2: structural basis of electromechanical coupling. *Science.* 309:903–908.

Long, S.B., X. Tao, E.B. Campbell, and R. MacKinnon. 2007. Atomic structure of a voltage-dependent K^+ channel in a lipid membrane-like environment. *Nature.* 450:376–382.

Lu, Z., A.M. Klem, and Y. Ramu. 2002. Coupling between voltage sensors and activation gate in voltage-gated K^+ channels. *J. Gen. Physiol.* 120:663–676.

MacArthur, M.W., and J.M. Thornton. 1991. Influence of proline residues on protein conformation. *J. Mol. Biol.* 218:397–412.

McCormack, K., M.A. Tanouye, L.E. Iverson, J.W. Lin, M. Ramaswami, T. McCormack, J.T. Campanelli, M.K. Mathew, and B. Rudy. 1991. A role for hydrophobic residues in the voltage-dependent gating of *Shaker* K^+ channels. *Proc. Natl. Acad. Sci. USA.* 88:2931–2935.

O'Neil, K.T., and W.F. DeGrado. 1990. A thermodynamic scale for the helix-forming tendencies of the commonly occurring amino acids. *Science.* 250:646–651.

Ohlenschlager, O., H. Hojo, R. Ramachandran, M. Gorlach, and P.I. Haris. 2002. Three-dimensional structure of the S4-S5 segment of the *Shaker* potassium channel. *Biophys. J.* 82:2995–3002.

Pathak, M.M., V. Yarov-Yarovoy, G. Agarwal, B. Roux, P. Barth, S. Kohout, F. Tombola, and E.Y. Isacoff. 2007. Closing in on the resting state of the *Shaker* K^+ channel. *Neuron.* 56:124–140.

Phillips, J.C., R. Braun, W. Wang, J. Gumbart, E. Tajkhorshid, E. Villa, C. Chipot, R.D. Skeel, L. Kale, and K. Schulten. 2005. Scalable molecular dynamics with NAMD. *J. Comput. Chem.* 26:1781–1802.

Rich, T.C., S.W. Yeola, M.M. Tamkun, and D.J. Snyders. 2002. Mutations throughout the S6 region of the hKv1.5 channel alter the stability of the activation gate. *Am. J. Physiol. Cell Physiol.* 282:C161–C171.

Sali, A., and T.L. Blundell. 1993. Comparative protein modelling by satisfaction of spatial restraints. *J. Mol. Biol.* 234:779–815.

Sanner, M.F., A.J. Olson, and J.C. Spehner. 1996. Reduced surface: an efficient way to compute molecular surfaces. *Biopolymers.* 38:305–320.

Scholle, A., T. Zimmer, R. Koopmann, B. Engeland, O. Pongs, and K. Benndorf. 2004. Effects of kv1.2 intracellular regions on activation of kv2.1 channels. *Biophys. J.* 87:873–882.

Tristani-Firouzi, M., J. Chen, and M.C. Sanguinetti. 2002. Interactions between S4-S5 linker and S6 transmembrane domain modulate gating of HERG K^+ channels. *J. Biol. Chem.* 277:18994–19000.

Yeola, S.W., T.C. Rich, V.N. Uebele, M.M. Tamkun, and D.J. Snyders. 1996. Molecular analysis of a binding site for quinidine in a human cardiac delayed rectifier K^+ channel. Role of S6 in antiarrhythmic drug binding. *Circ. Res.* 78:1105–1114.